Ultrafast electronic photoinduced phase transition in a two-dimensional charge-ordering system

K. Iwano

Graduate University for Advanced Studies, Institute of Materials Structure Science, High Energy Accelerator Research Organization (KEK), 1-1 Oho, Tsukuba 305-0801, Japan

(Received 22 June 2014; revised manuscript received 4 February 2015; published 3 March 2015)

We investigate the ground- and excited-state properties of a two-dimensional charge-ordering system, and theoretically demonstrate that multielectron excitations by one photon occur substantially as a result of frustration effects. These multielectron excitations are naturally regarded as domain excitations, which involve a simultaneous excitation of a part of the system lattice. Furthermore, we show that such domain excitations not only suppress the original charge-ordering phase strongly but also enhance another phase of charge ordering. As a result of such a global change, the overall photoinduced optical conductivity spectra are also modified drastically from the original spectrum, with the modified spectra exhibiting midgap and gapless features.

DOI: 10.1103/PhysRevB.91.115108 PACS number(s): 71.30.+h, 71.35.Lk, 78.20.Bh

I. INTRODUCTION

The physics of photoinduced phase transitions (PIPTs) has recently attracted increasing attention [1,2]. PIPTs are the phenomena in which a macroscopic phase change occurs with the trigger of photoexcitation in matter. One of our fundamental concerns is the mechanism of such phenomena, namely, elucidating why and how such a large change can occur. Traditionally, such phenomena have been attributed to structure-driven mechanisms [3–6]. These phenomena are characterized by large motions of constituent atoms, and hence they occur in time scales of typically picoseconds. Although the electronic states also change simultaneously, the process should be regarded as motion on a few adiabatic potential surfaces with the atomic structure being the main degrees of freedom.

In contrast to such *conventional* PIPTs, the existence of another possible type of PIPT has been hypothesized in the last decade. Namely, in some materials, the electronic change is expected to precede the atomic motion. The most transparent examples of such PIPTs can be observed in quasi-one-dimensional systems [7–10]. Theoretically, such behaviors have been naturally interpreted as an excitation of a quantum (electronic) domain. Such a domain is expected to grow in size rather easily, namely, without any further energy cost apart from the initial formation of a transition core that later becomes a domain-wall pair [11–14].

On the other hand, in the case of systems with higher dimensions, we encounter a theoretical difficulty. The essence of the difficulty is easily explained: the amount of the domain wall around a single domain, for example, the circumference of a circle in two dimensions, grows with the domain size. Consequently, we can naively infer that its formation energy inevitably increases for larger domain sizes. This diminishes the energy degeneracy among various domain states, which degeneracy is indispensable for the smooth growth of a domain of this type. Meanwhile, there is an experimental example that suggests the possibility of an ultrafast domain growth to a substantial size in two dimensions. The material is a so-called molecular solid, α-(BEDT-TTF)$_2$I$_3$, which exhibits a charge-ordered (CO) ground state at lower temperatures. It has been observed that a single absorbed photon converts approximately 250 molecules from the CO state to a CO-melted state [15] within a time interval of 25 fs [16,17]. This ultrafast time scale excludes the role of intermolecular lattice motions and certain low-frequency intramolecular vibrations such as intramolecular bendings since their time scales are typically slower than 1 ps, as expected from their vibrational frequencies of the order of 10 cm^{-1}. The remaining effect is the intramolecular stretchings, which have high frequencies comparable to electron transfer energies, although it is not the initial driving force but just follows the correlated electron motions [16]. The fact that such an ultrafast domain growth is realized in the actual material indicates the need for a more sophisticated theory to explain this growth. In this light, a previous study [18] has reported the observation of a metallic excited state in a high-energy region above the CO ground state, which appears to be related to the present concern, although the small system size (4×4) used in the study does not allow for a conclusive remark. We therefore try calculations on a larger system and investigate the possibility of the ultrafast domain growth.

This article is organized as follows. We give an introduction in this section, and the basic notions are explained in Sec. II. The method is explained in Sec. III and concrete results are described in Sec. IV. Section V is devoted to the concluding remark and discussions.

II. BASIC NOTIONS

In light of the above experimental finding, we theoretically investigate photoexcited states above the CO ground state. We first describe the selection of the model to describe the CO state. Although the actual material is considered to be a quarter-filled band system, we focus on the charge degrees of freedom and hence we adopt a spinless fermion model on a 6×6 lattice subject to the periodic boundary condition (PBC) and half electron filling. The model Hamiltonian is subsequently expressed as

$$H = -t_0 \sum_{\langle l,l' \rangle} (C_l^\dagger C_{l'} + \text{H.c.}) + \sum_{(l,l')} V(l-l') n_l n_{l'}, \quad (1)$$

where all of the operators operate on spinless fermions on a square lattice. To simplify calculations, we restrict the transfer term to the nearest-neighbor (nn) pairs $\langle l,l' \rangle$, and we denote its transfer energy by t_0. Meanwhile, the intersite repulsion

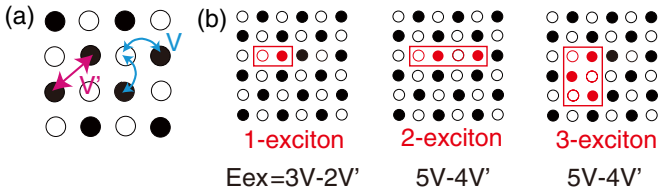

FIG. 1. (Color online) Schematics of (a) a part of the the checkerboard CO ground state with its considered repulsions and (b) three low-lying excited states in a 6×6 lattice.

term is slightly modified to include the next-nearest-neighbor (nnn) repulsion in addition to the nn one. Thus, the potential $V(l - l')$ is designated as V and V' for the former and the latter, respectively, as shown in Fig. 1(a). Here, we remark that the nnn repulsion is considered only for the diagonal pair of $l - l' = e_x + e_y$, with e_x and e_y denoting the two unit vectors of the square lattice. The last restriction is set to directly compare the present calculation with a preceding study on the ground state of the same Hamiltonian on a triangular lattice [19]. As is well known, such an addition to the repulsion causes the so-called checkerboard CO order depicted in Fig. 1(a) to become less stable. For example, an occupied nnn pair of sites in the above-mentioned direction costs extra V', which is nothing but a frustration as commonly observed in spin systems on a triangular lattice.

Meanwhile, in the excited states, this frustration is expected to uniquely influence their energetics. Figure 1(b) depicts certain low-lying excited states in the localized limit. When the repulsion is limited to the nn pairs, the excitation energy becomes $3V$ and $5V$ for the one-exciton and two- and three-exciton cases, respectively. We note that for another type of two-exciton case, namely, a squarelike one, its energy is $4V$ in this system. Furthermore, three-exciton cases of different shapes have the energies of $6V$ and $7V$. Thus, there is an overall tendency for the energy to increase as the number of excitons increases, which implies the disappearance of energy degeneracy among the domain states, as already mentioned above. In contrast, the situation drastically changes when we take frustration into account. As is specified in Fig. 1(b), the excitation energies are subtracted by the contributions from V', and the energy in all three cases reduces to V when V equals V', which corresponds to the phase boundary in the localized limit. Thus, we can expect a certain amount of degeneracy among the domain states, although certain domain states are excluded from achieving degeneracy because of shape and symmetry reasons. In this light, we mention that the significance of degeneracy in the triangular lattice is also discussed in Ref. [20], with regard to the transfer of doped carriers and their possible fractionalization.

III. METHOD

In this section, we explain the observable that we focus on, in the context of methodology. It has been reported that the photoinduced effect or, more explicitly, the photoinduced change in the reflectance spectrum is proportional to the light intensity [15]. This implies the scenario that a single absorbed photon creates one electronic domain of substantial size in a literal meaning. This scenario makes investigations based on the linear optical spectrum meaningful, and this approach forms the focus of this work. When compared with the direct calculation of the system's time evolution, this approach provides the advantage of examining a large part of the Hilbert space at one time. The regular part of the optical conductivity for x-polarized light measured at the ground state is subsequently calculated by means of the standard formula as

$$\sigma_{\rm reg}(\omega) = \frac{\gamma}{\omega} \sum_{n \neq g} \frac{|\langle n|j_x|g\rangle|^2}{(\omega - E_n + E_g)^2 + \gamma^2}, \tag{2}$$

where $|g\rangle$ and E_g denote the ground state and its eigenenergy, respectively, $|n\rangle$ and E_n denote those for any state n, j_x denotes the current operator in the x direction, and γ is the width of artificial broadening.

In practical calculations, we determine the ground state by using the Lanczos method [21], and we obtain the spectral shape by using the continued-fraction method [22]. The nature of each excited state is subsequently analyzed through the imaginary part of the so-called correction vector, which is defined as

$$\mathrm{Im}|x\rangle \equiv \mathrm{Im}\left(\frac{1}{H - E_g - \omega + i\gamma} j_x|g\rangle\right), \tag{3}$$

since this component accounts for the states with an excitation energy of approximately ω, and it is calculated by using the conjugate-gradient method [21].

Before describing the details of the calculations, we mention their two features. First, we have particular interest in the number of electron excitations, $N_{\rm ex}$, i.e., the number of excitons. From Fig. 1, while it might appear that determining this number is simple, there are at least two problems that we encounter in its determination. In this light, we propose a method of counting and explain it in Appendix A. As regards the second feature, we set a restriction for the number of states in the Hilbert space. In short, we set an upper bound for the number of occupied bonds as 14, except for cases explicitly mentioned. These details are described in Appendix B.

IV. RESULTS

A. Ground-state properties

As the first result, we discuss the ground-state properties found for the present system size. The overall properties of the system have already been discussed using a smaller system size [19], and those results are reproduced in Fig. 2(a), although we modify phase I considering compatibility with the present system size. We subsequently choose several parameter sets specified by the dots in Fig. 2(a) and evaluate the charge correlations expressed as $C(k_x, k_y) = (1/N)\sum_{l,l'} \langle n_l n_{l'}\rangle e^{ik_x(l_x - l_{x'}) + k_y(l_y - l_{y'})}$ with $N = 36$, as shown in Figs. 2(b) and 2(c) separately. Note that the quantities are calculated by the diagonalization using the full Hilbert space for Fig. 2(b), while the diagonalization is restricted up to the states with $N_{\rm bond} = 14$ because of limited computer resource. In spite of the restriction, we observe that the present results are closely consistent with the previous one [19]. In particular, the substantial increase for $k = (2/3\pi, 2/3\pi)$ makes a contrast to

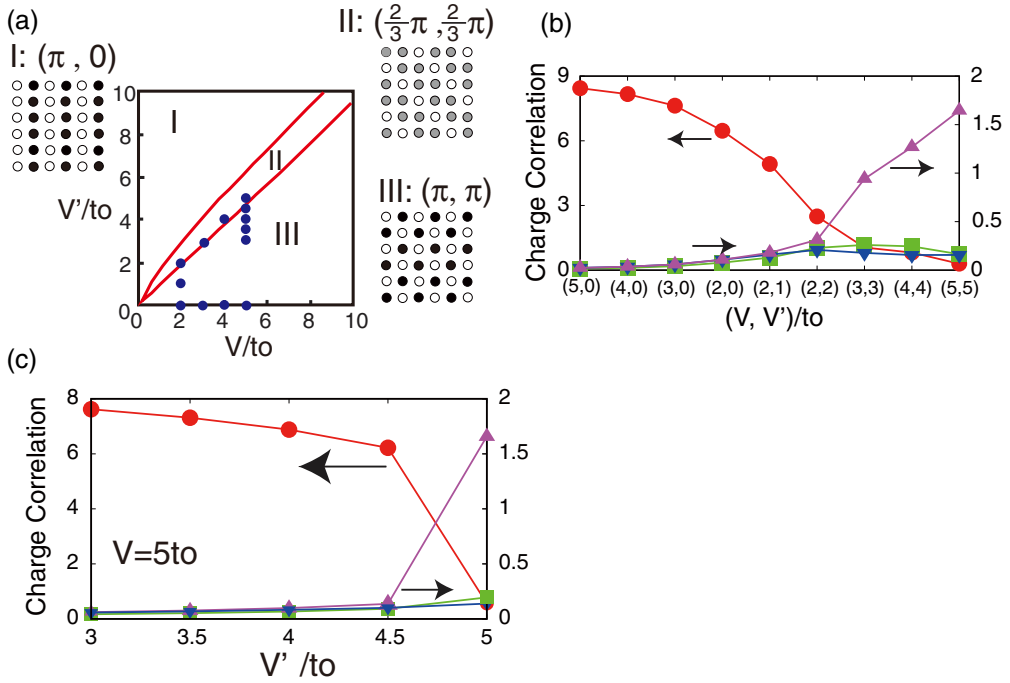

FIG. 2. (Color online) (a) Phase diagram reproduced from Ref. [19] along with the corresponding CO patterns in each region. It is noted that phase I is substituted by the $(\pi,0)$ phase because of compatibility with the 6×6 system size and that the gray circles in the pattern for phase II represent 0.75 electrons per site. (b),(c) Charge correlations for the sets of (V,V') specified by the dots in (a). Circles, squares, upward triangles, and downward triangles correspond to the results for $(k_x,k_y) = (\pi,\pi)$, $(\pi,0)$, $(2/3\pi,2/3\pi)$, and $(2/3\pi,-2/3\pi)$.

another diagonal direction, i.e., $k = (2/3\pi,-2/3\pi)$, which is a natural consequence of the present choice of the nnn repulsion.

B. Weak-coupling case

We next study the optical conductivity spectra calculated for the ground states that maintain the checkerboard type of CO. Here, we focus on cases with relatively small V and V'. According to the preceding studies [18,23], the magnitudes of the actual transfer energies are rather distributed over the range of ∼0.03–0.18 eV, depending on the types of bonds, whereas the V and V' values are estimated to be 0.35 and 0.3 eV, respectively. Although we do not intend a one-to-one correspondence, we then assume the V value as $2t_0$ and change the V' value within the checkerboard CO region.

Figure 3 shows the spectra obtained for $\gamma = 0.1t_0$ along with the energy-dependent $N_{\rm ex}$ values, although the latter appear as discrete values in the interest of saving on computer time. First, the upper-left panel for $(V,\ V')/t_0 = (2,0)$ shows the case with no frustration. The large peak around $5t_0$ is due to the one-exciton case that is depicted in Fig. 1(a), which fact is substantiated by the value of $N_{\rm ex}$ being close to 1 at the peak. The region corresponding to $N_{\rm ex} \sim 1$ including this peak extends to the second peak around $8t_0$, while we observe another small region with $N_{\rm ex} \sim 1$ around $10t_0$ and interpret it as due to a free electron-hole pair. In between these peaks, we observe a region characterized by $N_{\rm ex}$ values larger than three, and we attribute this region to a cluster of excitons, i.e., a domain state, although the spectral intensity is not so large, as shown by the hatching in Fig. 3(e) as an enlarged version of Fig. 3(a). We speculate that this is because the multiexciton states in Fig. 1(b) are not sufficiently degenerate with the one-exciton state in the absence of the V' term. We then add the nnn repulsions; the corresponding results are shown in Figs. 3(b)–3(d). From the hatchings for the $N_{\rm ex}$ curves, we observe the formation and growth of an additional region with increase in the V' value, accompanied by substantial spectral intensities. We attribute this to the emergence of domain states that are connected to the one-exciton state with appreciable matrix elements originating from t_0. In relation to the spectra, we also remark on size dependency. The patterns appearing in Fig. 11 of Appendix C correspond to three- and six-exciton states, and both of these states have energies of $6V - 6V'$ in the localized picture. These values are artificially reduced for the present system size with the PBC. For $(V,\ V')/t_0 = (2,1)$, for instance, this value equals $6t_0$, which falls in the region with the hatching. A possibility that the hatched area of the spectrum originates from such states might arise here. For this possibility, we think that this is not the case. Namely, the hatched area grows from around $\omega/t_0 \sim 6$–7 for $(V,\ V')/t_0 = (2,0.5)$, which is considerably smaller than the expected energy $6V - 6V' = 9t_0$, even if we take the energy lowering due to the itineracy into consideration.

To further understand the nature of the domain states, we also analyze the charge correlations for the states obtained as the correction vectors for each energy. Since the states appear to be smeared out in the case of $(V,\ V')/t_0 = (2,2)$, we choose the case of (2, 1) and depict the results in Fig. 4. We notice an overall suppression in the $C(\pi,\pi)$ correlation. Since the electron excitations from the checkerboard CO

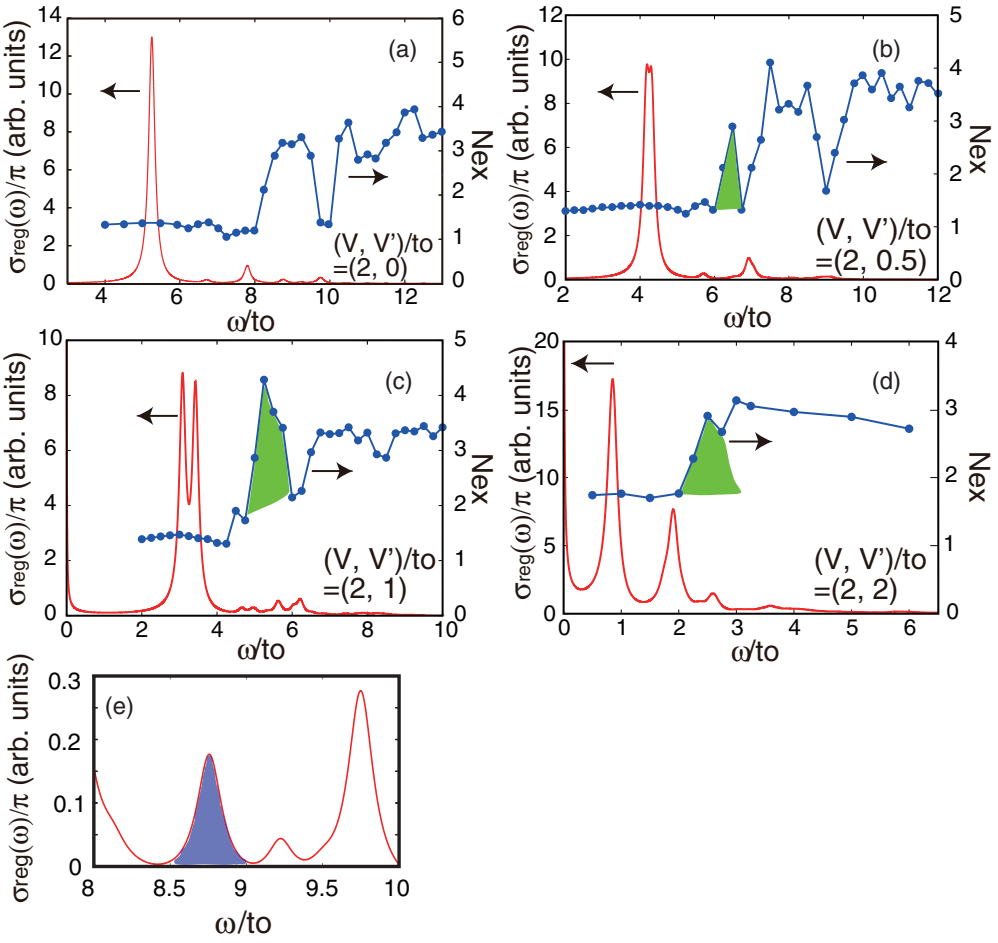

FIG. 3. (Color online) (a)–(d) Optical conductivity spectrum and energy-dependent N_{ex} values for four sets of (V, V') in the weak-coupling case and (e) a spectrum that enlarges a part of (a).

inevitably destroy the order, it is natural that its curve is almost an inversion of the corresponding N_{ex} curve appearing in Fig. 3(c). In particular, around $\omega = 5t_0$, we find a large degree of suppression due to the domain states that we have already mentioned. The reduced charge correlation is almost 20% of that of the original CO, which indicates that the order is drastically weakened by one-photon excitation with such energy. We next focus on the two correlations, $C(2\pi/3,2\pi/3)$ and $C(2\pi/3,-2\pi/3)$. As already discussed, the former relates to the CO of phase II, while the latter does not relate to any possible order. From these results, we observe a meaningful enhancement in the former when it is compared with the latter and subsequently speculate that another state similar to phase II is partially realized as a result of the excitations. As another comparison, we also focus on the result for the $C(\pi,0)$ correlation in Fig. 4. The enhancement appears to be of the same order as that for $C(2\pi/3,-2\pi/3)$, thereby suggesting no development of phase I. We attribute this lack of development to a finite "distance" of the present parameter set to phase I in the phase diagram.

As the last result of this section, we discuss the spectral features of the excited states in order to clarify the interplay among the excited states themselves. We use the expressions for the excited-state optical conductivity proposed in a preceding study [24], which expressions are explicitly mentioned in Appendix D. Here, we emphasize that we substitute the appropriate eigenstates and eigenenergies into Eqs. (D1)–(D3), which are obtained from the correction vector after checking the reliance as described in Appendix E. In fact, these expressions are justified for an eigenstate because they are based on the so-called Gell-Mann and Low theorem [25]. In Fig. 5(a), the eigenvalues thus obtained and measured from the ground-state energy are shown as a function of input ω for one of the previous cases, that is, $(V, V')/t_0 = (2,1)$. Using these energies E_{ex} as the excitation energies, we draw the photoinduced optical conductivity spectrum $\sigma_1(\omega)$ in Figs. 5(b) and 5(c). Here, we avoid the discussion of the Drude weight itself because its understanding requires the analysis of size dependencies, which is rather difficult for the excited states at this stage. As the first remark for the spectra, even for the lowest-energy excitation in Fig. 5(b), we observe a strong modification from the original spectrum $\sigma(\omega)$. In particular, the features of the original spectrum disappear almost completely apart from the bleaching at E_{ex}, which feature indicates the "soft" nature of the present system. Such a soft nature manifests itself more conspicuously for the domain excitations. For example, in Fig. 5(c), we observe further modifications in the spectrum, and the concentration of the

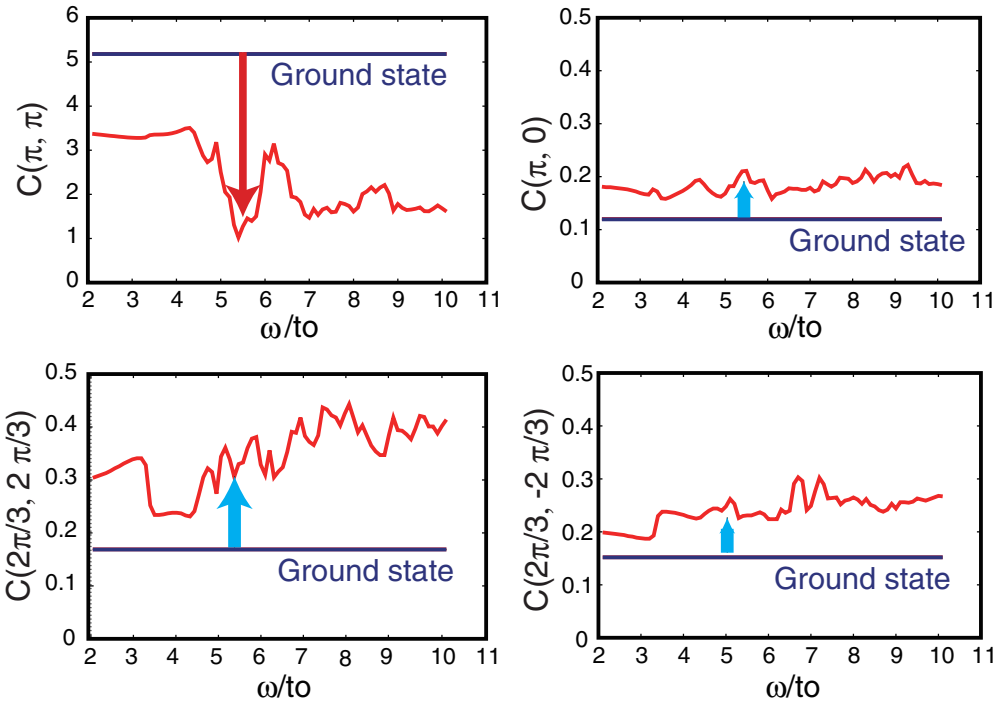

FIG. 4. (Color online) Energy-dependent charge correlations for $(V, V')/t_0 = (2,1)$. In each panel, the ground-state value is specified by the horizontal line.

spectral intensities in the very-low-energy region is the most conspicuous, in which the gapless feature suggests the metallic property of the domain states in this energy region.

C. Strong-coupling case

We next discuss the case with relatively large V and V' values. As was already mentioned in the previous section,

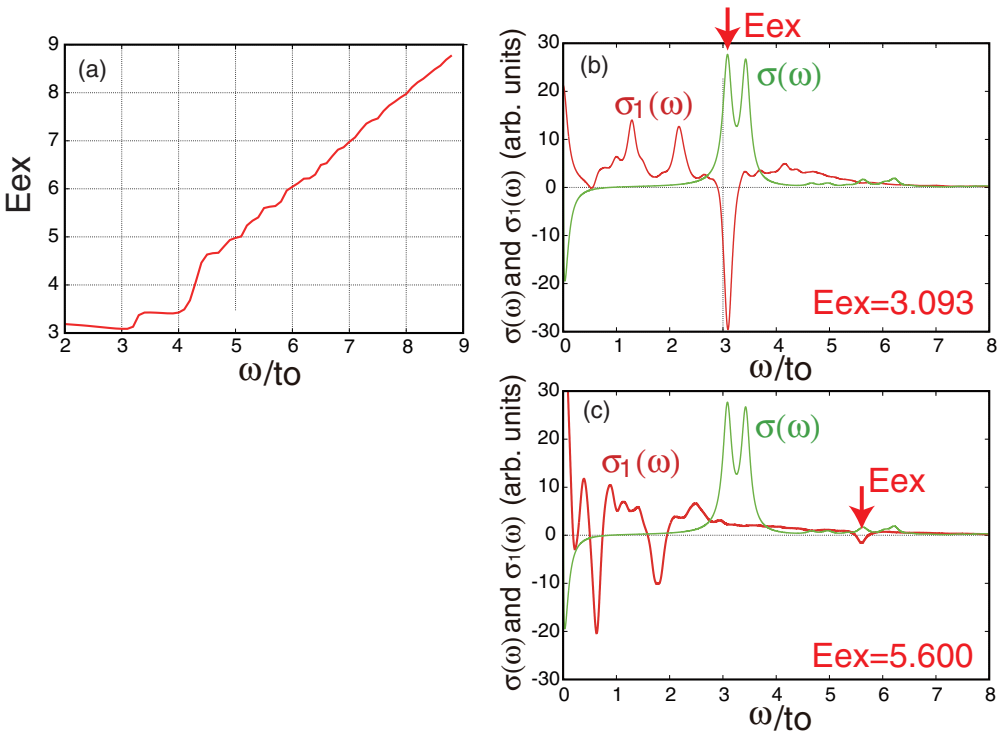

FIG. 5. (Color online) (a) Determined eigenenergies measured from the ground-state energy as a function of the input frequency, and (b),(c) photoinduced spectrum $\sigma_1(\omega)$ with the spectrum from the ground state, $\sigma(\omega)$, for $(V, V')/t_0 = (2,1)$. (b),(c) The excitation energy is specified by the vertical arrow.

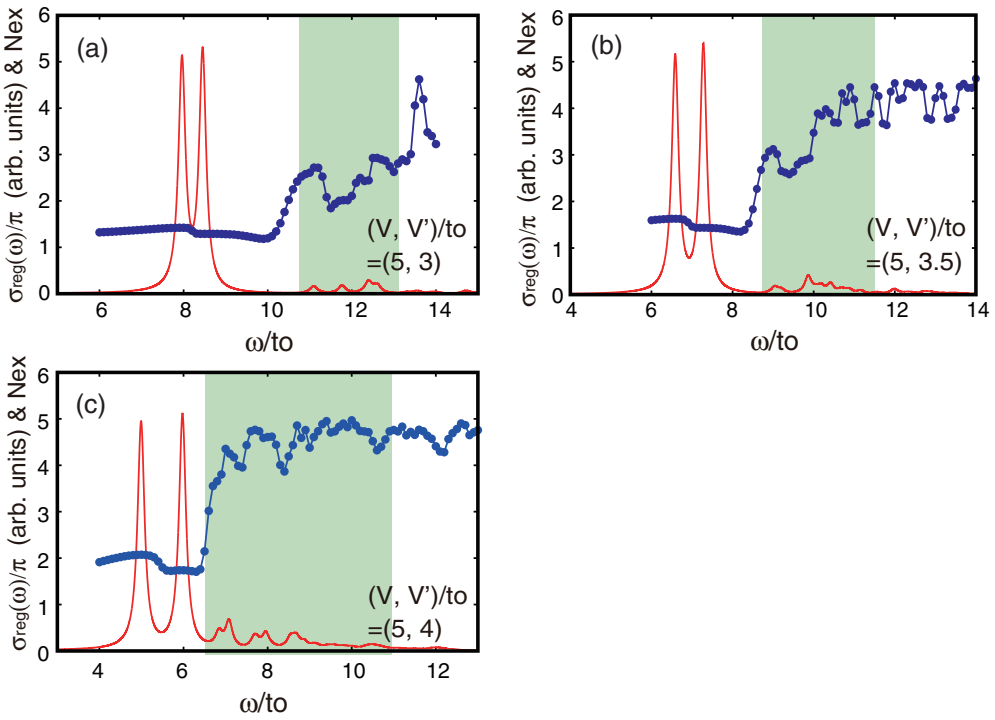

FIG. 6. (Color online) Optical conductivity spectrum and energy-dependent N_{ex} values for three sets of (V, V') in the strong-coupling case.

the parameter values appropriate for the actual material seem to belong to a weak-coupling case. Meanwhile, the present counting method for the electron number of excitations has a tendency to underestimate the number in the weak-coupling case, since all of the states including the ground state are hybridized strongly and make the nature of the excitations seared out. We therefore treat a strong-coupling case for the purpose of presenting the nature of the domain states more clearly.

In Fig. 6, we show the optical-conductivity spectra with the energy-dependent number of electron excitations, N_{ex}, as defined in the weak-coupling case. In these results, the V' value is changed for the fixed V value, i.e., $5t_0$, and all of the ground states exhibit the checkerboard CO as shown in Fig. 2(c). When

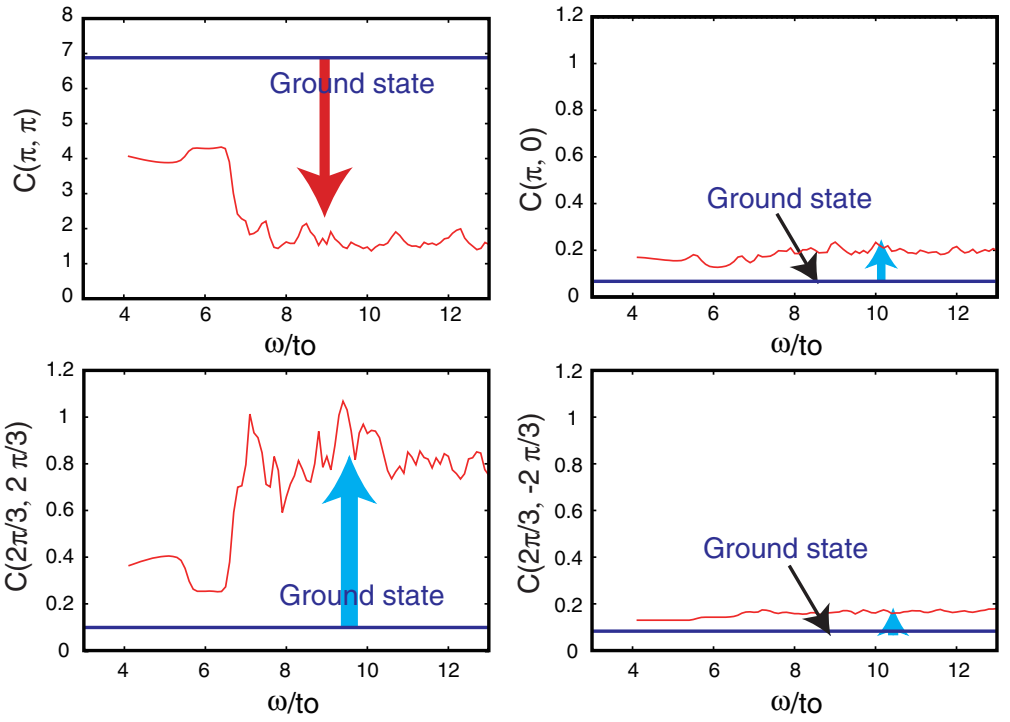

FIG. 7. (Color online) Same as Fig. 4, but for $(V, V')/t_0 = (5,4)$.

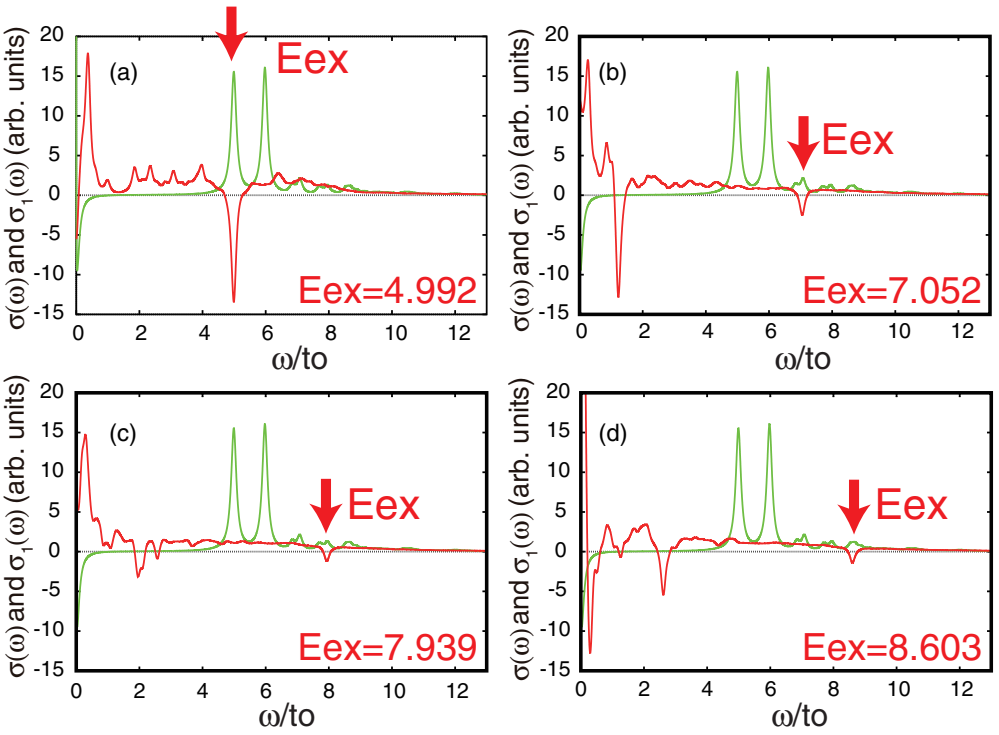

FIG. 8. (Color online) Photoinduced spectra for $(V, V')/t_0 = (5,4)$.

we increase the value of V' toward the phase boundary, the higher-energy tail in the hatched area not only becomes more conspicuous in intensity but also has larger N_{ex} values, which nearly reach five for $(V, V')/t_0 = (5,4)$. This behavior, which emerges more clearly than that in the weak-coupling case, is considered to originate from the strong-coupling nature. Regarding the states appearing in Fig. 11, their estimated energy, $6V - 6V'$, which is $12t_0$, $9t_0$, and $6t_0$, for Figs. 2(a)–2(c), respectively, resides inside the hatched area for Fig. 2(a), while it resides on its boundary for Fig. 2(b) and outside it for Fig. 2(c). Although we do not completely deny contributions from the states in Fig. 11, we judge that the hatched area originates mainly from the other size-independent states.

Such nature is also observed in the charge correlations in Fig. 7. Focusing on the case of $(V, V')/t_0 = (5,4)$, we first notice a large reduction in the charge conjugation $C(\pi,\pi)$ for the hatched area and small overall increases in $C(\pi,0)$ and $C(2\pi/3,-2\pi/3)$, as in the weak-coupling case. Meanwhile, the charge correlation for $C(2\pi/3,2\pi/3)$ exhibits a drastic increase in the region corresponding to the hatched area in Fig. 6(c), which behavior is interpreted as essentially the same as that in the weak-coupling case but as more enhanced due to the strong-coupling nature.

Lastly, we discuss the photoinduced spectra in the strong-coupling case, with $(V, V')/t_0 = (5,4)$ as an example. The results for four typical excitation energies are shown in Fig. 8. First, for the lowest excitation in Fig. 8(a), we also confirm midgap features similar to those in Fig. 5(b), although the features in Fig. 8(a) suggest the enhanced many-body nature of the excitation, being consistent with the larger N_{ex} values that exceed two. By increasing the excitation energy up to the hatched region in Fig. 6(c), namely, domain states, we observe that the gapless features become more conspicuous, which tendency again suggests the metallic nature of the domain states, although we reserve a conclusive remark about the metallicity because of the difficulty in the determination of the size dependencies of the Drude weight.

V. CONCLUSIONS

We have found that domain excitations accompanied by multielectron excitations and a consequent rearrangement of the original CO order around the domains can occur when we include frustration effects. Meanwhile, there are several aspects of such systems that require further investigation. First, the number of electron excitations, N_{ex}, for the domain excitations is still smaller than the observed number. In this regard, we speculate that larger system sizes and more sophisticated modeling including both long-range repulsions and transfers will solve it. Next, the use of real-time simulations can shed light on the multiphoton effect that manifests itself as a cooperative effect possibly working among the domains and relaxations within the excited states that are related to time domains after the very early stage. The roles of the spin degrees of freedom also require investigation, since we determined that the spin arrangements inside a domain determine its growth dynamics at least in one dimension [14]. We believe that such investigations in the near future will further clarify the nature of the PIPT as an electronic transition and aid in increasing our understanding of this interesting dynamical process.

ACKNOWLEDGMENTS

The research was carried out under the aegis of the Large Scale Simulation Program No. 11 (FY2013-2014) of KEK. A part of the simulation was performed on a supercomputer

(NEC SX9) at the Research Center for Nuclear Physics, Osaka University. The author appreciates valuable experimental information on this material from Professor S. Iwai. The author also appreciates valuable theoretical information from Professor S. Ishihara and Dr. H. Hashimoto and also expresses his thankfulness for innumerable advice related to numerical calculations from Dr. H. Matsufuru.

APPENDIX A: DEFINITION OF THE NUMBER OF ELECTRON EXCITATIONS

As is mentioned in the main text, there are two problems that make a simple counting difficult. One originates from the doubly degenerate ground states for this type CO, namely, those related to each other by the particle-hole exchange. The low-lying excited states as appearing in Fig. 1(b) are very naturally counted as one- to three-electron excitations, while it is rather subtle from which ground state a state is excited in the case of a large number of excitations because of the finite system size. Another difficulty is related to the ground-state fluctuation, namely, virtual excitations, which is rather large in some cases. We then propose the following way of counting and define the number of excitations to solve these problems practically.

The number of electron excitations, $N_{\rm ex}$, is calculated as the difference between the expectation values of a special operator $\hat{N}_{\rm ex}$ for the ground and the excited state, considering virtual excitations in the former, and is expressed as $N_{\rm ex} \equiv \langle ix|\hat{N}_{\rm ex}|ix\rangle - \langle g|\hat{N}_{\rm ex}|g\rangle$. Here, we use Im$|x\rangle$ in Eq. (3) as $|ix\rangle$ after normalization. The definition of $\hat{N}_{\rm ex}$ also needs some careful treatment because the counting of electron excitations depends on from which localized ground state as shown in Fig. 9 we count them. We thus take the policy of avoiding overestimation as much as possible, and use the following definition:

$$(\hat{N}_{\rm ex})_\mu \equiv {\rm Min}[(N_{\rm ex1})_\mu,(N_{\rm ex2})_\mu], \tag{A1}$$

where the index μ specifies each site-diagonal basis set, and the two quantities inside the parentheses are defined, using localized charge occupancies $n(i_x,i_y)$ at the (i_x,i_y) site, as

$$(N_{\rm ex1})_\mu \equiv \frac{1}{2}\sum_{i_x,i_y}\left|n(i_x,i_y)_\mu - \frac{1-(-1)^{i_x+i_y}}{2}\right| \tag{A2}$$

and

$$(N_{\rm ex2})_\mu \equiv \frac{1}{2}\sum_{i_x,i_y}\left|n(i_x,i_y)_\mu - \frac{1+(-1)^{i_x+i_y}}{2}\right|. \tag{A3}$$

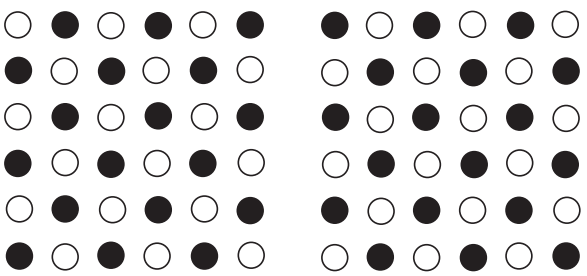

FIG. 9. Two ground states of the checkerboard CO in the localized picture.

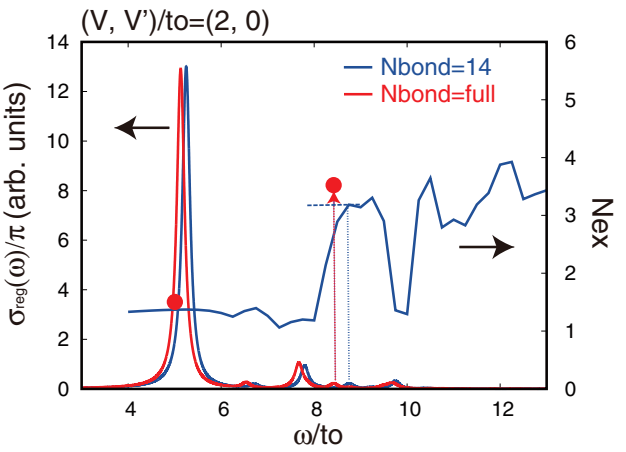

FIG. 10. (Color online) Comparisons between the result based on the full calculation and that with $N_{\rm bond} = 14$. They are obtained for $(V,V')/t_0 = (2,0)$. Closed circles specify the values of $N_{\rm ex}$ at those points.

APPENDIX B: RESTRICTION OF THE HILBERT SPACE DIMENSION USING $N_{\rm bond}$

While the full calculation that sets no limit restriction to the Hilbert space requires a huge memory as large as 4 TB, computer resources available are rather limited. Also, it takes a relatively long time to make the calculation of the correction vector converge to the accuracy that gives a reliable $N_{\rm ex}$ value. By the way, this calculation also gives a spectral intensity, which is a good check of the reliability since the continued fraction also gives the same quantity and the two values must coincide. In practical calculations, a restriction is done by setting an upper limit for the number of "occupied bonds," in which both of the connected sites are occupied. For example, the upper limit, which we denote $N_{\rm bond}$, is zero in the localized ground state, and three, five, five, for the one-, two-, and three-exciton states, respectively, as is easily seen in Fig. 1(b). By the way, the maximum $N_{\rm bond}$ is 30 in the present system size. Meanwhile, we often set it at a smaller number, i.e., 14, which reduces the dimension of the Hilbert space to almost one-tenth.

Below we give a result of the full calculations obtained so far and compare it with that assuming $N_{\rm bond} = 14$. Figure 10 is the result obtained for $(V,V')/t_0 = (2,0)$. In the figure, the two spectra are drawn together, and the value of $N_{\rm ex}$ is obtained only for two frequencies in the case of the full calculation.

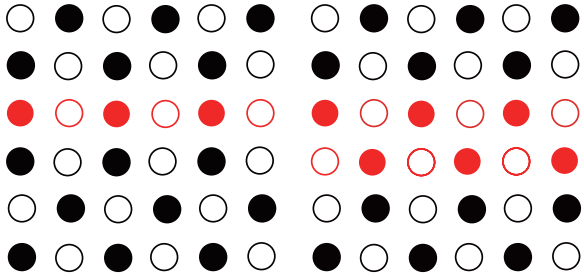

FIG. 11. (Color online) Two patterns that have $6V-6V'$ as the excitation energy in the localized picture.

There are quantitative differences between the result of the full calculation and that with $N_{\rm bond} = 14$. We, however, judge that the results give the qualitatively same tendencies although the latter tends to underestimate the effect of the multiexciton excitations, and rely on the calculation with $N_{\rm bond} = 14$ in the results explained in the main text.

APPENDIX C: PATTERNS THAT ARE EXPECTED TO HAVE SMALLER EXCITATION ENERGIES THAN THOSE IN AN INFINITE LATTICE

In Fig. 11, we show patterns that have $6V$–$6V'$ as the excitation energy in the localized picture. As is easily seen, these types of excitations have higher energies in the infinite lattice system, namely, $7V$–$6V'$ and $8V$–$7V'$, for the left and right patterns, respectively.

APPENDIX D: DEFINITION OF THE OPTICAL CONDUCTIVITY AT THE EXCITED STATE

Following the definition in the preceding study, [24] we use the following expression for the optical conductivity for the excited states themselves:

$$\sigma_1(\omega) = D_1\delta(\omega) + \sigma_1^{\rm reg}(\omega) + \sigma_1^{\rm reg'}(\omega)\ , \tag{D1}$$

where

$$\sigma_1^{\rm reg}(\omega) = -\frac{1}{\omega}{\rm Im}\left[\langle ex|j_x\frac{1}{(\omega - H + E_{\rm ex}) + i\gamma}j_x|ex\rangle\right]$$
$$= \frac{\gamma}{\omega}\sum_{n\neq ex}\frac{|\langle n|j_x|ex\rangle|^2}{(\omega - E_n + E_{\rm ex})^2 + \gamma^2}, \tag{D2}$$

$$\sigma_1^{\rm reg'}(\omega) = \frac{1}{\omega}{\rm Im}\left[\langle ex|j_x\frac{1}{(\omega + H - E_{\rm ex}) + i\gamma}j_x|ex\rangle\right]$$
$$= -\frac{\gamma}{\omega}\sum_{n\neq ex}\frac{|\langle n|j_x|ex\rangle|^2}{(\omega + E_n - E_{\rm ex})^2 + \gamma^2}, \tag{D3}$$

and

$$D_1 = 2\pi\left(-\frac{1}{4}\langle ex|K|ex\rangle - \sum_{n\neq ex}\frac{|\langle n|j_x|ex\rangle|^2}{E_n - E_{\rm ex}}\right), \tag{D4}$$

with K and $|ex\rangle$ being the kinetic part of the Hamiltonian (1) and the obtained eigenstate.

APPENDIX E: HOW TO FIND EIGENENERGIES AND EIGENVECTORS

The imaginary part of the corrections vector defined in Eq. (3) is basically described as a linear combination of different eigenvectors, although it is expected to approximate an eigenvector when the frequency ω comes sufficiently close to an eigenenergy. We hence inspect each imaginary part of the correction vector and consider it as an eigenvector if it passes a criterion. As the actual procedure, we first normalize the imaginary part of the correction vector in Eq. (3). Denoting it as $|ix\rangle$, we estimate the excitation energy of the eigenenergy associated with it as

$$E_{\rm ex} = ||H|ix\rangle|| - E_g, \tag{E1}$$

where $||\cdot||$ is the norm of the vector inside. After this, we evaluate the overlap between the two vectors, which are $|ix\rangle$ and $H|ix\rangle/(E_g + E_{\rm ex})$. If the former is a good approximation of an eigenvector, this overlap is expected to be close to unity. In practical calculations, we set the lower limit for this overlap as 0.9999.

[1] *Relaxations of Excited States and Photoinduced Structural Phase Transitions*, edited by K. Nasu, Springer Series in Solid State Science, Vol. 124 (Springer-Verlag, Berlin, 1997).
[2] K. Yonemitsu and K. Nasu, Phys. Rep. **465**, 1 (2008).
[3] Y. Toyozawa, Physica **117B & 118B**, 23 (1983).
[4] E. Hanamura and N. Nagaosa, J. Phys. Soc. Jpn. **56**, 2080 (1987).
[5] Y. Toyozawa, Solid State Commun. **84**, 255 (1992).
[6] S. Koshihara and S. Adachi, J. Phys. Soc. Jpn. **75**, 011005 (2006), and references therein.
[7] H. Okamoto, Y. Ishige, S. Tanaka, H. Kishida, S. Iwai, and Y. Tokura, Phys. Rev. B **70**, 165202 (2004).
[8] S. Iwai, Y. Ishige, S. Tanaka, Y. Okimoto, Y. Tokura, and H. Okamoto, Phys. Rev. Lett. **96**, 057403 (2006).
[9] H. Matsuzaki, M. Yamashita, and H. Okamoto, J. Phys. Soc. Jpn. **75**, 123701 (2006).
[10] K. Kimura, H. Matsuzaki, S. Takaishi, M. Yamashita, and H. Okamoto, Phys. Rev. B **79**, 075116 (2009).
[11] N. Nagaosa and J. Takimoto, J. Phys. Soc. Jpn. **55**, 2745 (1986).
[12] K. Iwano, Phys. Rev. Lett. **97**, 226404 (2006).
[13] M. Mayr and P. Horsch, Phys. Rev. B **73**, 195103 (2006).
[14] K. Iwano, Phys. Rev. Lett. **102**, 106405 (2009).
[15] S. Iwai, K. Yamamoto, A. Kashiwazaki, F. Hiramatsu, H. Nakaya, Y. Kawakami, K. Yakushi, H. Okamoto, H. Mori, and Y. Nishio, Phys. Rev. Lett. **98**, 097402 (2007).
[16] Y. Kawakami, T. Fukatsu, Y. Sakurai, H. Unno, H. Itoh, S. Iwai, T. Sasaki, K. Yamamoto, K. Yakushi, and K. Yonemitsu, Phys. Rev. Lett. **105**, 246402 (2010).
[17] S. Iwai (private communication). According to the latest experimental measurement, the time scale is 25 fs.
[18] H. Gomi, A. Takahashi, T. Tatsumi, S. Kobayashi, K. Miyamoto, J. Lee, and M. Aihara, J. Phys. Soc. Jpn. **80**, 034709 (2011).
[19] C. Hotta, N. Furukawa, A. Nakagawa, and K. Kubo, J. Phys. Soc. Jpn. **75**, 123704 (2006).
[20] C. Hotta and F. Pollmann, Phys. Rev. Lett. **100**, 186404 (2008).
[21] Y. Saad, *Iterative Methods for Sparse Linear Systems*, 2nd ed. (Society for Industrial and Applied Mathematics, Philadelphia, 2003).
[22] E. R. Gagliano and C. A. Balseiro, Phys. Rev. Lett. **59**, 2999 (1987).
[23] S. Miyashita and K. Yonemistu, J. Phys. Soc. Jpn. **77**, 094712 (2008).
[24] N. Maeshima and K. Yonemistu, J. Phys. Soc. Jpn. **74**, 2671 (2005).
[25] M. Gell-Mann and F. Low, Phys. Rev. **84**, 350 (1951).